Efficient and reliable strategy for identifying muon sites based on the double adiabatic approximation

THE JOURNAL OF PHYSICAL CHEMISTRY C

Article

pubs.acs.org/JPCC

Efficient and Reliable Strategy for Identifying Muon Sites Based on the Double Adiabatic Approximation

P. Bonfà, F. Sartori, and R. De Renzi*

Dipartimento di Fisica e Scienze della Terra, Parco Area delle Scienze 7/A, I-43124 Parma, Italy

ABSTRACT: We revise the simple and yet powerful approach of the Double Adiabatic Approximation (DAA) to study positive muon embedding sites in condensed matter. This method introduces a tractable and reasonably accurate description of the quantum nature of the muon in Density Functional Theory (DFT) simulations aiming at identifying muon sites. Moreover, this approach overcomes the limitations of the harmonic approximation in terms of both computational efforts and accuracy. Notably, it also improves treatment of muon diffusion. We use the DAA and Nudged Elastic Band calculations to determine the muon sites and the activation energies between equivalent sites in MnSi and copper. In metallic Cu, the proposed phonon-assisted mechanism for the low-temperature muon diffusion in the lattice is confirmed.

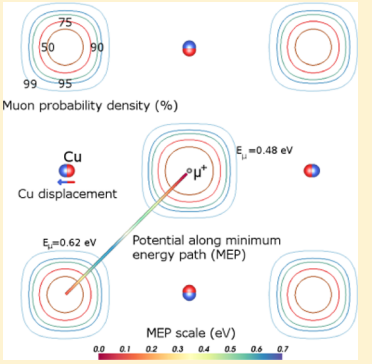

INTRODUCTION

Muon spin rotation and relaxation (μSR) spectroscopy is an experimental technique that provides the time evolution of the muon spin polarization by exploiting the anisotropic emission of the decay positron.

The main field of application of μSR is material science, but it is also adopted in chemistry for studying molecular dynamics and radical kinetics.[1−3] Both μ^-SR and μ^+SR exist, but, since μ^- undergoes nuclear capture and the surviving μ^- fall into atomic orbitals extremely close to the nuclei, μ^+SR is more commonly used to investigate condensed matter.

μSR experiments provide a measure of the microscopic field distribution at the interstitial site(s) where the μ^+ stop inside the sample. A seemingly embarrassing point is that these sites are usually unknown to the experimenter and the additional lack of knowledge on the perturbation generated locally by the positive muon probably represent the most common criticisms of the experimental technique. Even though in a large variety of cases ignoring the muon position does not represent a limitation, having access to information on interstitial sites and on muon-induced perturbations might be crucial to evaluate electronic properties such as long-range magnetic orders or localized magnetic moments.

Predicting the position of interstitial muon sites is not a trivial task. During the final stages of thermalization in the sample the scattering between the muon and the atoms of the compound leads to a kinetic energy degradation from hundreds to tenths of electronvolts. Nonetheless, the identification of diamagnetic muon sites with approaches based on the Density Functional Theory (DFT) is emerging as a new and valuable strategy to routinely assist μSR experiments interpretation. After the pioneering work of Van de Walle et al., in recent years, this method, which provides information on the electronic and crystalline perturbations introduced by the muon, has been validated in many experimental cases with great success.[4−13]

There are two main difficulties in the DFT approach. One is inherited from the mean-field description which cannot always correctly describe some classes of materials, like strongly correlated electrons systems or even some semiconductors mistaken for metals. This problem can be alleviated with the many ad hoc corrections that have been developed so far.[14−18] The second problem arises from the omission of the quantum nature of the nuclei. In standard DFT simulations, the nuclei are treated with the usual Born−Oppenheimer (BO) approximation in order to solve two separate Schrödinger equations for the nuclei and for the electrons. The BO approximation represents one of the major drawbacks in the description of the muon/sample interactions since the muon enters as a (light) proton in the Kohn−Sham Hamiltonian, which is self-consistently solved only for the electrons. When modeling the effect of the impurity, one usually finds many metastable configurations that turn out to be unstable when the kinetic energy of the muon is taken into account.

Motivated by the study of muon vibrational energies or proton coupled transfer reactions, many approaches to go beyond the BO scheme have been developed.[19−29] However, since our aim is to provide a supporting tool for μSR data analysis (as it is already the case for many other spectroscopic techniques), these methods are found to be prohibitively demanding of storage and computer time. For this reason the quantum nature of the muon, which is of course relevant given its small mass, is introduced a posteriori.[8,30]

Received: December 17, 2014
Revised: January 30, 2015

DOI: 10.1021/jp5125876
J. Phys. Chem. C XXXX, XXX, XXX−XXX

A method already used in this context is the linear response approach to study the vibrational modes of the muon impurity in the hosting material.[8,31] This strategy has the advantage of treating the muon and the nuclei on the same footing and uses the usual BO separation for the electrons. This is reasonable in view of the small ratio between the proton mass and the muon mass. However, it is known that, even for the protons, the harmonic approximation can break down.[32] Of course, this is usually the case also for the muon. For this reason we recovered a different approach based on the Double Adiabatic Approximation (DAA) which has already been used for both the proton and the muon to study their ground state energy.[23,30] While its applicability is limited to materials having heavy nuclei, starting from magnesium the ratio $m_{Mg}/m_\mu \sim 214$ exceeds m_μ/m_e, making the electronic BO separation the main source of approximation. Moreover, as discussed below, this approach has the additional advantage of providing a rough but cost-effective analysis of the diffusion mechanisms which can take place after muon's thermalization.[33−38]

The article is divided as follows. In the next section we briefly summarize our DFT approach to identify muon sites and report the DAA equations for clarity. Then we present two examples which illustrate the advantages of using the DAA method for studying the ground state energy of the muon.

MUON SITE IDENTIFICATION WITH DFT

The main idea, introduced by many works so far,[6−9,11,13] is to consider the positive diamagnetic muon as a hydrogenoid impurity in the system under study. The relaxed positions for the charged impurity are then identified by sampling the interstitial space with a grid of points in the unit cell and minimizing the forces in the system for each of the starting positions. This kind of simulations are usually performed with periodic boundary conditions, therefore supercells are constructed to limit the contribution arising from the interaction of the impurity with its periodic replica. It has been found that a neutral supercell approach provides the best results for metals, while a charged supercell with a corresponding compensating background is a better approximation for insulators.[6−8,10] This is understood by considering that in metals the charged particle is effectively screened by conduction electrons and the neutral supercell approach is therefore a better description of the real system.

During the above minimization procedure, many local minima are occasionally encountered. We label them "candidate muon sites". Usually not all candidate sites are muon sites. This is due to the quantum nature of the muon which is neglected in the relaxation steps. This problem is not so relevant when studying hydrogen intercalation since small energy barriers are sufficient to trap hydrogen impurities. However, the ground state energy of the muon can be up to an order of magnitude larger than that of the proton, thus making many interstitial positions unstable. To discriminate between binding and nonbinding sites, the ground state energy of the muon must be evaluated.

Incidentally, we remark that the quantum description of the muon also provides relevant information on phenomena such as muon diffusion or hyperfine couplings.[5,8]

DOUBLE ADIABATIC APPROXIMATION

As already discussed, a quantum description of the muon can be introduced by studying its vibrational modes. However, apart from accuracy problems, the number of irreducible modes that have to be analyzed grows with the number of basis elements within the simulation cell. Since treating the muon as an impurity requires a supercell approach, this method often becomes extraordinarily demanding even for the most powerful supercomputers.

Here we propose instead to introduce a double adiabatic approximation to separate the degrees of freedom of the muon from those of the electrons and of the nuclei. This is a rather crude approximation in some cases, but it has at least three valuable advantages. First, it allows to take into account the potential felt by the muon beyond the harmonic approximation. Second, this method can provide ground state energies for unrelaxed structures. This is especially useful when studying diffusion processes as will be discussed later. Finally, this approach provides information on the muon wave function with a reasonable amount of computational effort.

We now briefly recall the DAA equations for a single muon in the sample. The total Hamiltonian of the system is

$$\mathcal{H}_{tot} = -\frac{\hbar^2}{2m_\mu}\nabla_\mu^2 - \sum_{j=1}^{N_N}\frac{\hbar^2}{2M_j}\nabla_{N_j}^2 + \mathcal{H}_e \quad (1)$$

$$\mathcal{H}_e = -\sum_{i=1}^{N_e}\frac{\hbar^2}{2m_e}\nabla_i^2 + V(\mathbf{r}_e, \mathbf{r}_\mu, \mathbf{R}) \quad (2)$$

$$\mathcal{H}_{tot}|\Psi\rangle = E|\Psi\rangle \quad (3)$$

where index j runs over the N_N nuclei having the set of position operators $\mathbf{R}$ and masses M_j, $\mathbf{r}_\mu$, and m_μ are the position operator and the mass of the muon and the index i runs over the N_e electrons having the set of coordinate operators $\mathbf{r}_e$ and mass m_e and $V(\mathbf{r}_e, \mathbf{r}_\mu, \mathbf{R})$ includes all the interactions between the electrons, the nuclei and the muon. If we approximate the total wave function $|\Psi\rangle$ with the product wave function $|\psi_e\rangle|\phi_\mu\rangle|\chi_N\rangle$, the position operators of the muon and of the nuclei enter only as parameters in the eigenvalue problem for the electrons $\mathcal{H}_e\psi_e(\mathbf{r}_e; \mathbf{r}_\mu, \mathbf{R}) = \epsilon(\mathbf{r}_\mu, \mathbf{R})\psi_e(\mathbf{r}_e; \mathbf{r}_\mu, \mathbf{R})$ that is solved with the Kohn−Sham iterative scheme. By solving the Schrödinger equation of the electrons for the positions $\{\mathbf{r}_\mu\}$ we can construct the potential entering the Schrödinger equation of the muon:.

$$\left(-\frac{\hbar^2}{2m_\mu}\nabla_\mu^2 + \epsilon(\mathbf{r}_\mu, \mathbf{R})\right)\phi_\mu(\mathbf{r}_\mu; \mathbf{R}) = E_\mu(\mathbf{R})\phi_\mu(\mathbf{r}_\mu; \mathbf{R}) \quad (4)$$

Let $E_\mu^{(i)}$ be the i-th eigenvalue of eq 4, in the following we will refer to $E_i = E_\mu^{(i)}(\mathbf{R}) - \min_{r_\mu}[\epsilon(\mathbf{r}_\mu, \mathbf{R})]$ as the i-th energy of the i-th muon eigenfunction ($i = 0$ being the ground state).

At a first sight it may seem that this approach is rather impractical since it requires the execution of a large number of self-consistent loops. However, the intermediate mass of the muon greatly reduces the number of points to be acquired. Indeed the ground state energy of the muon is usually slightly less than 1 eV. This makes the calculation feasible since it is possible to obtain a good accuracy up to a couple of eV by interpolating a points cloud formed by 5 to 10 hundred points. The favorable convergence against the supercell sizes (usually less than 100 atoms are required) and the constantly increasing computational power available on computer clusters make this method effective for many materials.

DOI: 10.1021/jp5125876
J. Phys. Chem. C XXXX, XXX, XXX−XXX

EXPLORATION ALGORITHM

Cutting the computational costs needed to acquire the potential felt by the muon is of utmost importance. To this aim it is necessary to optimize the sampling process used to construct the points cloud on which the interpolation is performed. Acquiring all points in a cubic grid would probably result in a too expensive computational procedure. Moreover, only a small subset of the points acquired with this strategy could eventually be used to interpolate the potential of eq 4 since interstitial positions close to the nuclei have rapidly increasing total energies ϵ. Finally, as discussed in the next sections, the potential felt by the muon is usually far from being harmonic, thus, making the sampling over a sphere of increasing radius similarly inefficient.

A simple exploration algorithm was designed to perform an efficient sampling of the a priori unknown potential felt by the muon. The exploration is controlled by three parameters: a cutoff energy ϵ_C, a grid separation length δ, and a "search horizon" Δ. The first parameter is used to specify the highest energy that should be explored. The second parameter governs the interspacing between explored points in a cubic grid. The third parameter controls the maximum distance between two consecutively examined points during the exploration process. This last parameter is essential for two reasons. First and especially in magnetic materials, the previously calculated electron density must be used to converge to the correct ground state and avoid other local minima in the total energy landscape which reproduce, for example, different magnetic configurations. This can be done only if the impurity is not too far from the position where the previous self-consistency was obtained. Second, reuse of electron densities speeds up the calculation significantly.

The algorithmic procedure begins with the definition of the starting point for the exploration (labeled i) and the evaluation of its total energy ϵ_i. Let $n(i)$ be the number of neighboring points of point i in a cubic grid for which the total energy has not been calculated yet (in the implementation used in this article we considered only the nearest neighbors: left, right, up, down, front, back). From the initial point, the iteration proceeds as follows:

- The total energies of the neighboring points $n(i)$ of the current point i are inspected.
- The number of unexplored neighbors $n(i)$ for all explored points i is updated.
- Among the already explored points j, those with $n(j) > 0$ form the set of the candidate positions for the next move. The point j having the lowest energy ϵ_j and having distance $d(i,j) < \Delta$ is chosen as the next point for the exploration.
- The current position is set to position j and the algorithm is iterated.

The iteration stops when there are no points j fulfilling the conditions $n(j) > 0$, $d(i, j) < \Delta$, and $\epsilon_j < \epsilon_C$.

For $\Delta = \infty$ (infinite "search horizon") all points with $\epsilon < \epsilon_C$ will be explored. This is no longer true when we limit the maximum distance between consecutively explored points since the algorithm can remain trapped in dead-end paths. To avoid this situation we can imagine to label visited points with three different colors: red, explored points whose energy exceeds the cutoff energy, $\epsilon > \epsilon_C$; yellow, explored points having $\epsilon < \epsilon_C$ and at least one neighbor unexplored; green, explored points without unexplored neighbors.

When a dead-end point is reached, there are two possible scenarios: either none of the explored points is yellow or there is at least one yellow point. In the first case, the exploration is finished, otherwise, we move from point k, where the system is trapped, to the nearest yellow point, l. If reuse of electron density is required, the path that minimizes the distance $d(k,l)$, obtained for example with the algorithm by Klein and co-workers,[39] can be used in order to reduce the additional computational cost of traversing already explored points.

At the present stage, it is up to the user to check if the set of explored points can accurately interpolate the potential up to the threshold that is required for the subsequent analysis.

Starting from the points cloud $\{\epsilon(\mathbf{r}_\mu)\}$, the potential V_μ is obtained by interpolation with radial basis function (RBF) interpolants and with the Quadratic Shepard method.[40−42]

In what follows we will refer to the above algorithm as Potential Exploration Algorithm (PEA).

COMPUTATIONAL DETAILS

The DFT simulations were performed with the QUANTUM ESPRESSO suite of codes.[43] The PEA code is built on top of the routines of PW.X.

In all the calculations shown hereafter, we used the GBRV pseudopotential library and the generalized gradient approximation (GGA) as parametrized by Perdew−Burke−Ernzerhof (PBE) to describe the exchange-correlation potential.[44,45] The self-consistency threshold for electronic optimization was set to $\leq 10^{-8}$ Ry. For relaxation calculations, in order to reach convergence, two conditions had to be met: less than 10^{-3} Ry/Bohr for forces and total energy differences between relaxation steps smaller than 10^{-4} Ry. The Broyden−Fletcher−Goldfarb−Shanno (BFGS) algorithm has been used for structural optimization.

To locate the saddle points and optimize the transition path between equivalent muon sites, we performed Nudged Elastic Band (NEB) calculations.[46,47] To comply with the DAA approximation, we kept the atoms of the compound fixed in their relaxed positions in all the images of the NEB simulations. This gives an upper bound for the saddle point energy between equivalent muon sites. In all NEB calculations, the convergence threshold was set to 0.05 eV/Å for the forces normal to the path.

MANGANESE SILICIDE

The muon site in ferromagnetic MnSi has been thoroughly studied in a recent experiment by Amato and co-workers.[48] A single muon site is identified with high accuracy using transverse field μSR measurements of the dipolar tensor in the paramagnetic state. For this reason, MnSi represents an ideal test-case for our computational scheme.

The candidate muon sites were identified by performing structural relaxations on a 64 atoms MnSi supercell plus the muon impurity. We used a cutoff of 60 and 400 Ry for plane waves expansion and for the charge density respectively and a 2 × 2 × 2 Monkhorst−Pack (MP) grid for reciprocal space sampling.[49] Spin polarization was included in all simulations. With these parameters the total energy was converged to 15 meV. Four starting points were selected to sample the interstitial space in the unit cell. Their positions together with the symmetry replica are shown in Figure 1. We find three candidate muon sites which are reported in Table 1.

DOI: 10.1021/jp5125876
J. Phys. Chem. C XXXX, XXX, XXX−XXX

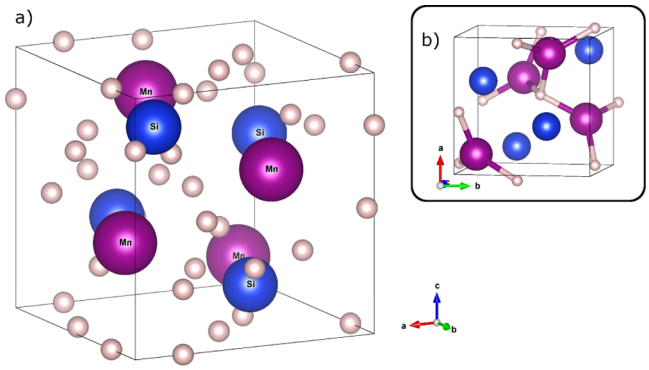

Figure 1. (a) Interstitial points (together with the symmetry replica) used as starting positions for the identification of the candidate muon sites. (b) Stable site found in MnSi (some equivalent sites outside the unit cell are shown to help the comparison with Figure 2b,c).

Table 1. Candidate Muon Sites Obtained with Structural Relaxations in a 64 + 1 Atoms Supercell[a]

candidate sites	position	$\epsilon^{(i)} - \epsilon^{(A)}$ (eV)	$E_0^{(i)}$ (eV)
A	(0.542, 0.542, 0.542)	0	0.6
B	(0.607, 0.477, 0.220)	0.86	
C	(0.329 0.329, 0.329)	1.12	

[a] $\epsilon^{(i)}$ is the total energy of the relaxed structure, $E_0^{(i)}$ is the ground state energy of the muon (see eq 4). The Mn and Si positions in the unperturbed cubic lattice are assumed at (0.1381, 0.1381, 0.1381) and (0.8462, 0.8462, 0.8462), respectively. The experimentally identified muon site is in fractional coordinates (0.532, 0.532, 0.532).

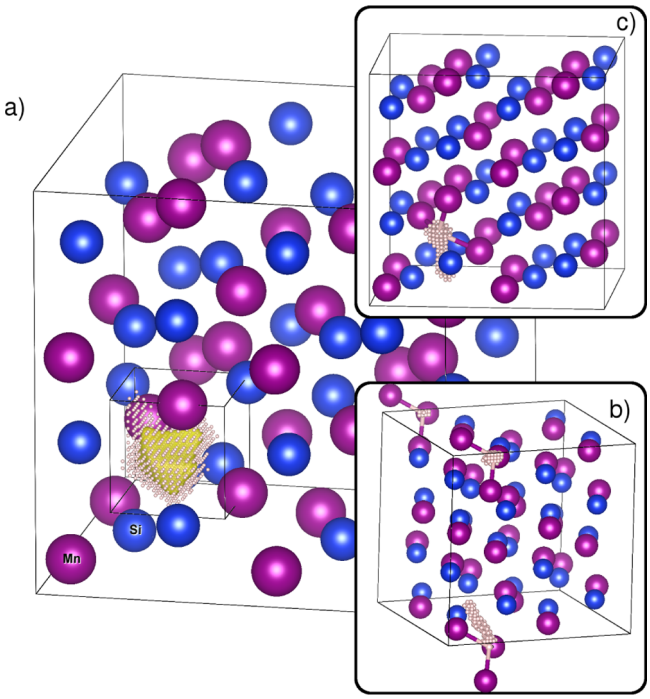

Figure 2. Main panel (a) shows the potential felt by the muon in the DAA approximation and the points cloud used for the interpolation. The isosurface is at 0.8 eV. (b, c) Small dots identify some of the points acquired, with the exploration algorithm described in the text starting from sites B and C, which are found to be local minima and nontrapping sites. In both cases, site A (see Table 1) is reached.

We checked if candidate muon sites are binding sites with the DAA approximation. For the sake of speed, in the PEA simulations we slightly reduced the accuracy of the calculation by lowering to 50 and 250 Ry the kinetic energy and charge expansions and sampling the Brillouin zone using only the Baldereschi point.[50] This guarantees a convergence of the total energy of ∼0.5 meV/atom. While the total energy convergence may seem poor, we checked the accuracy of the differences between the relaxed and the displaced positions energies by performing calculations with higher cutoff and a 2 × 2 × 2 MP sampling grid for reciprocal space. These tests were done for the first 20 points of the PEA calculation and for other random points. The worst case discrepancy was 4 meV with an average value of 1.5 meV. The spacing δ = 0.15875 Å was used for the cubic grid and the maximum step length between consecutive moves was set to $3\sqrt{3}\delta$.

Sites B and C are local minima in V (r_μ) and the barrier toward site A, which in both cases is lower than 0.15 eV, is too small to bind the muon.

Starting from site A, 827 points provide an accurate sampling of the potential up to 1.13 eV. The points cloud shown in Figure 2a is used for the interpolation and the Schrödinger equation for the muon is solved in a 2.54 Å edge cubic box with both Dirichlet and periodic boundary conditions. From the solution of the Schrödinger equation we obtain a ground state energy E_0 = 0.6 eV (independently of the interpolation method and the boundary conditions used). The probability density of the ground state wave function (not shown) is well localized and, by considering the concept of turning point volume,[6] the same conclusion can be drawn from Figure 2a, where even the isosurface for V_μ = 0.8 eV is found to be confined inside the points cloud acquired during the simulation.

It should be noted that $E_0^{(A)}$ is smaller than what it is reported by Amato et al.[48] This is because in our previous paper we provided preliminary results obtained by solving the Schrödinger equation for the muon in the unperturbed electrostatic potential. The disagreement between the two approaches is not surprising since in the latter case the electrons are frozen in the unperturbed ground state density.

From these results we can conclude that only one muon site is present in MnSi. This is in agreement with the experimental outcomes and the position obtained from the simulation differs from the experimental estimation by less than 0.05 Å.[48]

COPPER

Face-centered cubic copper represents an interesting test case since it is known that the muon diffuses through the material with a correlation time τ_c which, in the temperature range from 100 to 300 K, follows an exponential law and ranges from τ_c^{-1} ∼0.1 to 10 μs^{-1}.[35] The diffusion mechanism was thoroughly studied with both experimental and theoretical approaches.[36,51−54] In one of the last experiments performed on highly pure FCC copper samples, the high temperature data could be fitted with both a classical thermal activated law, that is, $\tau_c^{-1} \propto \exp(-E_A/k_BT)$ (E_A activation energy to overjump the barrier) and a phonon-mediated tunneling model that takes into account the small polaron theory.[55,56] In the latter case, a temperature-dependent prefactor multiplies the exponential law.[51,57] Above 300 K, a few experimental data points seem to completely miss the 90−300 K and Schilling et al.[51] and Teichler[57,58] suggested that, at high temperature, an additional diffusion mechanism should take place.

Here we checked if the DAA approach is sufficiently accurate to allow the description of the diffusion mechanism(s). The

DOI: 10.1021/jp5125876
J. Phys. Chem. C XXXX, XXX, XXX−XXX

identification of the muon site followed the standard procedure described above. A cubic supercell with 32 Cu atoms and the muon was considered. Two candidate positions in the octahedral (O) and the tetrahedral (T) cavity sites were correctly identified with the structural relaxations. In the T and O sites, the nearest neighboring Cu atoms are outward displaced from the muon by 5.9 and 2.3%, respectively. The latter value is slightly smaller than what is experimentally observed, but it is in agreement with previous calculations.[52,59] The same result is also obtained with a 109 atom cell, thus, confirming the convergence against the supercell size.

We collected the points needed to interpolate V_μ with PEA calculations performed with cutoffs of 50 and 250 Ry for the plane wave and the charge density expansion respectively and a $3 \times 3 \times 3$ MP grid for reciprocal space integration. The same spacing δ used for MnSi was adopted. Starting from the T site, the barrier toward O sites is just 0.3 eV and no localized states at the T site were found. The first 800 points acquired starting from the O site are shown in Figure 3b. As it is evident from the figure, during the exploration process the PEA reached the saddle point between the O and the T site, explored the T site and then moved to the equivalent O minimum of the neighboring cell.

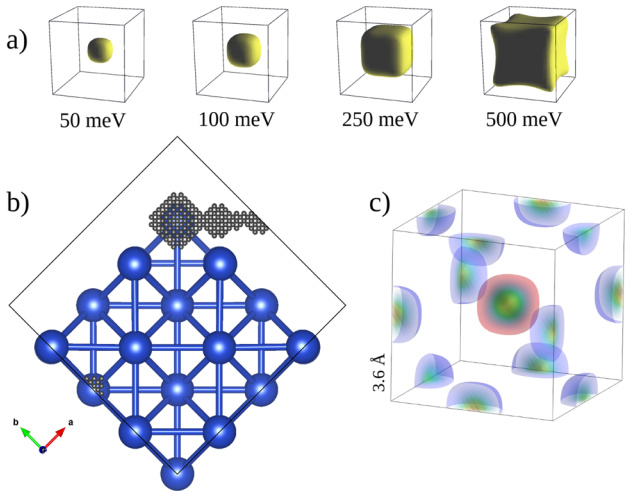

Figure 3. (a) Four isosurfaces for the interpolated potential felt by the muon in the octahedral site. Notice that at nuclear "phonon-like" energies, the potential almost retains its spherical shape. On the other hand, at muon vibration energies, the potential is far from being harmonic. (b) First 800 points acquired during the exploration with the PEA. Copper atoms are in blue, while all the positions occupied by the muon are in gray. The route toward the neighboring octahedral site passing through the tetrahedral site is clearly visible. Copper atoms do not appear at all the cell boundaries because of the small distortion introduced by the muon (see text). (c) Probability densities for the ground state and the degenerate excited states are depicted with a color map and the 95% probability densities are shown with red (central) and blue (corners) isosurfaces, respectively.

In conclusion, the O site is clearly the global minimum of V_μ and we can deduce that the muon hops among O sites only.[52]

To check if the mechanism responsible for the muon diffusion is the classical overbarrier hopping or a phonon-assisted quantum tunneling, the energy barrier between the O sites and the eigenstates for a muon in the distorted O site and in the neighboring sites must be evaluated.

By imposing the 48 point group symmetry operations on the acquired points, a 9301 points cloud was obtained and used to interpolate the potential of the distorted O site and of the 12 neighboring equivalent sites, providing an accurate description of the potential up to 1.5 eV. We then solved the Schrödinger equation for the muon in the potential V_μ, which is obtained by interpolation of the data points with radial basis functions (with r, r^3, and $r^2 \times \log(r)$ as basis functions) and trilinear interpolation with periodic boundary conditions.

We found a ground state with $E_0 \sim 0.48$ eV and degenerate excited states at $E_1 = 0.62$ eV (the results from the various interpolation schemes differ by about 10 meV). As shown in Figure 3c, the two energies correspond to a muon completely localized in the distorted O site and in the neighboring O sites, respectively. No states localized only in the T site were found for energies up to 1 eV.

To evaluate the overbarrier activation energy, the minimum energy path between equivalent O sites was calculated with NEB simulations. The results, obtained using the same parameters for reciprocal space integration and convergence criteria as for the PEA calculations, are shown in Figure 4. The curve is asymmetric due to the distortion introduced by the muon in the starting O site. The best path toward the neighboring O site passes through the T site. The saddle point energy between the O and the T site is at $E_{OT} = 0.56$ eV, while the one between two neighboring O sites is at about $E_{OO} = 0.66$ eV above the energy of the starting muon site. The same information can be directly extracted from the interpolated potential. The estimation of E_{OT} and E_{OO} extracted from the interpolated potential agrees to within 5 meV with the one obtained with the NEB approach. The path between O sites passing through a Cu−Cu bond has a much higher saddle point energy (about 1.6 eV).

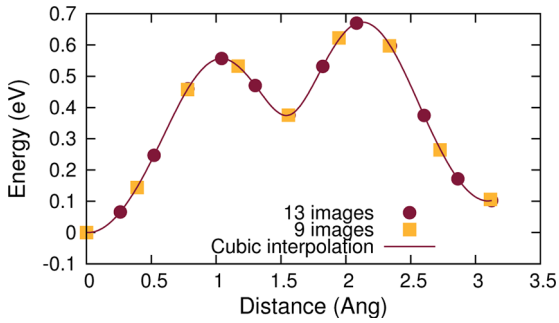

Figure 4. Minimum energy path between equivalent octahedral muon sites obtained with 13 and 9 images NEB simulations. The solid line, obtained from the cubic interpolation of the 13 images NEB results, is used to estimate the value of the saddle points' energy. The difference between the initial and the final energy is due to the distortion introduced by the muon in its starting site.

The energy difference $E_{OO} - E_1 \sim 40$ meV indicates that the phonon-assisted quantum tunneling dominates over the classical hopping at low temperature, that is, in the 80−300 K range. However, the classical diffusion mechanism should take place at slightly higher temperatures. Indeed, Schilling and co-workers found a better agreement of the experimental data with the phonon assisted small polaron diffusion theory and extracted an activation energy of about 80 meV.[51] The value found with the DAA is about 1.7 times larger, but this is probably an overestimation due to the adiabatic approximation.

DOI: 10.1021/jp5125876
J. Phys. Chem. C XXXX, XXX, XXX−XXX

DISCUSSION AND CONCLUSION

The main message of this paper is that an accurate analysis of the ground state energy of the muon (possibly beyond the harmonic approximation) allows to evaluate the stability of the numerous candidate muon sites that are provided by the structural relaxations. This can strikingly improve the predictive power of DFT simulations in providing muon embedding sites.

In this paper we discussed an efficient and yet sufficiently accurate method to obtain a quantum description of the muon. The PEA machinery provides a reliable way to distinguish between trapping and nontrapping muon sites (which are routinely obtained during the structural relaxations) with a computationally tractable description of the ground state energy of the muon. Moreover, differently from methods based on the analysis of the vibrational modes of the μ^+ impurity, this approach can provide eigenfunctions and energies for a muon in an unrelaxed neighborhood, thus allowing the analysis of quantum tunneling mechanisms. The estimation of the muon wave function can also produce accurate ab initio evaluations of many observables (e.g., contact and transferred hyperfine couplings).[8,30] While the applicability of the DAA is limited to the compounds having heavy nuclei, even the mass ratio m_μ/m_C is smaller than 1%.

The accuracy and the limits of the BO approximation have been extensively discussed in literature.[60−62] An encouraging result for the muon case in this context has been provided by Takahashi and Takatsuka who considered the accuracy of the BO approximation for the $pp\mu^-$ molecule (p stands for proton) and found a deviation smaller than 5% from the non-BO vibronic energies calculated with semiclassical methods.[63]

It should also be noted that for both MnSi and Cu the potential felt by the muon is far from being harmonic nor it is possible to fully describe it with small an-harmonic corrections as evidenced in Figure 2a and Figure 3a. This is the case for almost all the compound that we examined so far.

To verify the accuracy of the DAA, we had to revert to the comparison with the experiment. In doing so, we chose two nontrivial examples that have been thoroughly characterized experimentally. In MnSi, we found that the ground state energy of the muon makes two candidate sites unstable leaving only one trapping muon site per unit cell. The final site is in nice quantitative agreement with the measured muon position, which differs by less than 0.05 Å. In FCC copper, an accurate evaluation of the ground state energy of the muon allowed to distinguish between classical and phonon-mediated tunneling diffusion, providing slightly overestimated values for the activation energies, but correctly identifying a lower activation energy for the phonon-mediated mechanism, in agreement with the experimental data.

Moreover, even though in literature correct estimations of the muon sites were drawn from the analysis of the electrostatic potential in metals, these must be regarded as fortunate cases since they are based on crude and not well-justified assumptions. On the other hand, it is always possible to estimate the accuracy of the DAA approach by comparing the kinetic energies of the species forming the compound under study.

As a side remark, we add that the PEA code can also be used for studying proton vibrational energies in those compounds where the harmonic approximation is not sufficiently accurate. We tested some textbook cases (hydrogen compounds HRb and HI) and found that the DAA approach slightly improves the agreement with the experimental results.

We finally mention that the results shown in this article were obtained with a computational power ranging from 8 to 64 cores operating at clock speeds between 2.2 and 3 GHz. These performances are nowadays becoming available also on standalone workstations.

The source codes used for the PEA calculations, which include the potential exploration tool and the 1D and 3D Schrödinger equation solvers,[64,65] are published on the web.[66]

AUTHOR INFORMATION

Corresponding Author

*E-mail: roberto.derenzi@unipr.it.

Notes

The authors declare no competing financial interest.

ACKNOWLEDGMENTS

The authors thank computing resources provided by STFC's Scientific Computing Department and by Paul Scherrer Institute with the Merlin4 Cluster. We acknowledge financial support from PRIN Project 2012 × 3YFZ2. Special thanks are due to Johannes Möller, Franz Lang, Alex Amato, and Roberto Cammi for fruitful discussions.

REFERENCES

(1) Yaouanc, A.; Dalmas de Réotier, P. *Muon Spin Rotation, Relaxation, and Resonance: Applications to Condensed Matter*; International Series of Monographs on Physics; OUP: Oxford, 2011.

(2) Clayden, N. J. Muons in Chemistry. *Phys. Scr.* **2013**, *88* (068507), 1−10.

(3) Percival, P. W.; Addison-Jones, B.; Brodovitch, J.-C.; Ji, F.; Horoyski, P. J.; Thewalt, M. L. W.; Anthony, T. R. ^{13}C Hyperfine Coupling Constants in MuC_{60}. *Chem. Phys. Lett.* **1995**, *245*, 90−94.

(4) Van de Walle, C. G.; Denteneer, P. J. H.; Bar-Yam, Y.; Pantelides, S. Theory of Hydrogen Diffusion and Reactions in Crystalline Silicon. *Phys. Rev. B* **1989**, *39*, 10791−10808.

(5) Van de Walle, C. G. Structural Identification of Hydrogen and Muonium Centers in Silicon: First-Principles Calculations of Hyperfine Parameters. *Phys. Rev. Lett.* **1990**, *64*, 669−672.

(6) Bernardini, F.; Bonfà, P.; Massidda, S.; De Renzi, R. Ab Initio Strategy for Muon Site Assignment in Wide Band Gap Fluorides. *Phys. Rev. B* **2013**, *87* (115148), 1−7.

(7) Möller, J. S.; Bonfà, P.; Ceresoli, D.; Bernardini, F.; Blundell, S. J.; Lancaster, T.; De Renzi, R.; Marzari, N.; Watanabe, I.; Sulaiman, S.; et al. Playing Quantum Hide-and-Seek With the Muon: Localizing Muon Stopping Sites. *Phys. Scr.* **2013**, *88* (068510), 1−7.

(8) Möller, J. S.; Ceresoli, D.; Lancaster, T.; Marzari, N.; Blundell, S. J. Quantum States of Muons in Fluorides. *Phys. Rev. B* **2013**, *87* (121108), 1−5.

(9) Blundell, S. J.; Möller, J. S.; Lancaster, T.; Baker, P. J.; Pratt, F. L.; Seber, G.; Lahti, P. M. μSR Study of Magnetic Order in the Organic Quasi-One-Dimensional Ferromagnet F4BImNN. *Phys. Rev. B* **2013**, *88* (064423), 1−6.

(10) Prando, G.; Bonfà, P.; Profeta, G.; Khasanov, R.; Bernardini, F.; Mazzani, M.; Brüning, E. M.; Pal, A.; Awana, V. P. S.; Grafe, H.-J.; et al. Common Effect of Chemical and External Pressures on the Magnetic Properties of RCoPO (R = La, Pr). *Phys. Rev. B* **2013**, *87* (064401), 1−11.

(11) Disseler, S. M. Direct Evidence for the All-In/All-Out Magnetic Structure in the Pyrochlore Iridates From Muon Spin Relaxation. *Phys. Rev. B* **2014**, *89* (140413), 1−5.

(12) Mantz, Y. A.; Gemmen, R. S. Protonated Forms of Monoclinic Zirconia: A Theoretical Study. *J. Phys. Chem. C* **2010**, *114*, 8014−8025.

(13) Foronda, F. R.; Lang, F.; Möller, J. S.; Lancaster, T.; Boothroyd, A. T.; Pratt, F. L.; Giblin, S. R.; Prabhakaran, D.; Blundell, S. J.

DOI: 10.1021/jp5125876
J. Phys. Chem. C XXXX, XXX, XXX−XXX

Anisotropic Local Modification of Crystal Field Levels in Pr-Based Pyrochlores: A Muon-Induced Effect Modeled Using Density Functional Theory. *Phys. Rev. Lett.* **2015**, *114* (017602), 1−5.
(14) Levine, Z. H.; Allan, D. C. Linear Optical Response in Silicon and Germanium Including Self-Energy Effects. *Phys. Rev. Lett.* **1989**, *63*, 1719−1722.
(15) Gonze, X.; Lee, C. Dynamical Matrices, Born Effective Charges, Dielectric Permittivity Tensors, and Interatomic Force Constants From Density-Functional Perturbation Theory. *Phys. Rev. B* **1997**, *55*, 10355−10368.
(16) Anisimov, V. I.; Zaanen, J.; Andersen, O. K. Band Theory and Mott Insulators: Hubbard U Instead of Stoner I. *Phys. Rev. B* **1991**, *44*, 943−954.
(17) Petukhov, A. G.; Mazin, I. I.; Chioncel, L.; Lichtenstein, A. I. Correlated Metals and the LDA+U Method. *Phys. Rev. B* **2003**, *67* (153106), 1−4.
(18) Ortenzi, L.; Mazin, I. I.; Blaha, P.; Boeri, L. Accounting for Spin Fluctuations Beyond Local Spin Density Approximation in the Density Functional Theory. *Phys. Rev. B* **2012**, *86* (064437), 1−6.
(19) Miyake, T.; Ogitsu, T.; Tsuneyuki, S. Quantum Distributions of Muonium and Hydrogen in Crystalline Silicon. *Phys. Rev. Lett.* **1998**, *81*, 1873−1876.
(20) Valladares, R.; Fisher, A.; Hayes, W. Path-Integral Simulations of Zero-Point Effects for Implanted Muons in Benzene. *Chem. Phys. Lett.* **1995**, *242*, 1−6.
(21) Kerridge, A.; Harker, A. H.; Stoneham, A. M. Quantum Behaviour of Hydrogen and Muonium in Vacancy-Containing Complexes in Diamond. *J. Phys.: Condens. Matter* **2004**, *16*, 8743−8751.
(22) Gidopoulos, N. I.; Gross, E. K. U. Electronic Non-Adiabatic States: Towards a Density Functional Theory Beyond the Born-Oppenheimer Approximation. *Philos. Trans. R. Soc. A* **2014**, *372* (20130059), 1−9.
(23) Soudackov, A. V.; Hammes-Schiffer, S. Removal of the Double Adiabatic Approximation for Proton-Coupled Electron Transfer Reactions in Solution. *Chem. Phys. Lett.* **1999**, *299*, 503−510.
(24) Pak, M. V.; Hammes-Schiffer, S. Electron-Proton Correlation for Hydrogen Tunneling Systems. *Phys. Rev. Lett.* **2004**, *92* (103002), 1−4.
(25) Webb, S. P.; Iordanov, T.; Hammes-Schiffer, S. Multiconfigurational Nuclear-Electronic Orbital Approach: Incorporation of Nuclear Quantum Effects in Electronic Structure Calculations. *J. Chem. Phys.* **2002**, *117*, 4106−4118.
(26) Tachikawa, M.; Mori, K.; Nakai, H.; Iguchi, K. An Extension of Ab Initio Molecular Orbital Theory to Nuclear Motion. *Chem. Phys. Lett.* **1998**, *290*, 437−442.
(27) Nakai, H. Nuclear Orbital Plus Molecular Orbital Theory: Simultaneous Determination of Nuclear and Electronic Wave Functions Without Born-Oppenheimer Approximation. *Int. J. Quantum Chem.* **2007**, *107*, 2849−2869.
(28) González, S. A.; Aguirre, N. F.; Reyes, A. Theoretical Investigation of Isotope Effects: The Any-Particle Molecular Orbital Code. *Int. J. Quantum Chem.* **2008**, *108*, 1742−1749.
(29) Posada, E.; Moncada, F.; Reyes, A. Negative Muon Chemistry: The Quantum Muon Effect and the Finite Nuclear Mass Effect. *J. Phys. Chem. A* **2014**, *118*, 9491−9499.
(30) Porter, A. R.; Towler, M. D.; Needs, R. J. Muonium as a Hydrogen Analogue in Silicon and Germanium: Quantum Effects and Hyperfine Parameters. *Phys. Rev. B* **1999**, *60*, 13534−13546.
(31) Baroni, S.; de Gironcoli, S.; Dal Corso, A.; Giannozzi, P. Phonons and Related Crystal Properties From Density-Functional Perturbation Theory. *Rev. Mod. Phys.* **2001**, *73*, 515−562.
(32) Erba, A.; Casassa, S.; Dovesi, R.; Maschio, L.; Pisani, C. Periodic Density Functional Theory and Local-Mp2 Study of the Librational Modes of Ice XI. *J. Chem. Phys.* **2009**, *130* (074505), 1−9.
(33) Powell, A. S.; Lord, J. S.; Gregory, D. H.; Titman, J. J. Muon Spin Relaxation Studies of Lithium Nitridometallate Battery Materials: Muon Trapping and Lithium Ion Diffusion. *J. Phys. Chem. C* **2009**, *113*, 20758−20763.
(34) Gil, J. M.; Mendes, P. J.; Ferreira, L. P.; Alberto, H. V.; Vilão, R. C.; Ayres de Campos, N.; Weidinger, A.; Tomm, Y.; Niedermayer, C.; Yakushev, M. V.; et al. Modeling Hydrogen in $CuInSe_2$ and $CuInS_2$ Solar Cell Materials Using Implanted Muons. *Phys. Rev. B* **1999**, *59*, 1912−1916.
(35) Kadono, R.; Imazato, J.; Matsuzaki, T.; Nishiyama, K.; Nagamine, K.; Yamazaki, T.; Richter, D.; Welter, J.-M. Quantum Diffusion of Positive Muons in Copper. *Phys. Rev. B* **1989**, *39*, 23−41.
(36) Luke, G. M.; Brewer, J. H.; Kreitzman, S. R.; Noakes, D. R.; Celio, M.; Kadono, R.; Ansaldo, E. J. Muon Diffusion and Spin Dynamics in Copper. *Phys. Rev. B* **1991**, *43*, 3284−3297.
(37) Storchak, V. G.; Prokof'ev, N. V. Quantum Diffusion of Muons and Muonium Atoms in Solids. *Rev. Mod. Phys.* **1998**, *70*, 929−978.
(38) Kiefl, R. F.; Kadono, R.; Brewer, J. H.; Luke, G. M.; Yen, H. K.; Celio, M.; Ansaldo, E. J. Quantum Diffusion of Muonium in KCl. *Phys. Rev. Lett.* **1989**, *62*, 792−795.
(39) Klein, P. N.; Rao, S.; Raucht, M.; Subramanian, S. Faster Shortest-Path Algorithms for Planar Graphs. STOC'94 ACM Symposium on Theory of Computing, Montreal, QC, Canada, May 23−25, 1994, ACM: New York, 1994, 27−37.
(40) Franke, R. Scattered Data Interpolation: Tests of Some Methods. *Math. Comp.* **1982**, *38*, 181−200.
(41) Renka, R. J. Algorithm 661: QSHEP3D: Quadratic Shepard Method for Trivariate Interpolation of Scattered Data. *ACM Trans. Math. Softw.* **1988**, *14*, 151−152.
(42) Burkardt, J. Home Page. http://people.sc.fsu.edu/~jburkardt/ (accessed Jan. 26, 2015).
(43) Giannozzi, P.; Baroni, S.; Bonini, N.; Calandra, M.; Car, R.; Cavazzoni, C.; Ceresoli, D.; Chiarotti, G. L.; Cococcioni, M.; Dabo, I.; et al. QUANTUM ESPRESSO: A Modular and Open-Source Software Project for Quantum Simulations of Materials. *J. Phys.: Condens. Matter* **2009**, *21* (395502), 1−19.
(44) Garrity, K. F.; Bennett, J. W.; Rabe, K. M.; Vanderbilt, D. Pseudopotentials for High-Throughput DFT Calculations. *Comput. Mater. Sci.* **2014**, *81*, 446−452.
(45) Perdew, J. P.; Burke, K.; Ernzerhof, M. Generalized Gradient Approximation Made Simple. *Phys. Rev. Lett.* **1996**, *77*, 3865−3868.
(46) Weinan, E.; Ren, W.; Vanden-Eijnden, E. String Method for the Study of Rare Events. *Phys. Rev. B* **2002**, *66* (052301), 1−4.
(47) Henkelman, G.; Jónsson, H. A Dimer Method for Finding Saddle Points on High Dimensional Potential Surfaces Using Only First Derivatives. *J. Chem. Phys.* **1999**, *111*, 7010−7022.
(48) Amato, A.; Dalmas de Réotier, P.; Andreica, D.; Yaouanc, A.; Suter, A.; Lapertot, G.; Pop, I. M.; Morenzoni, E.; Bonfà, P.; Bernardini, F.; et al. Understanding the μSR Spectra of MnSi Without Magnetic Polarons. *Phys. Rev. B* **2014**, *89* (184425), 1−10.
(49) Monkhorst, H. J.; Pack, J. D. Special Points for Brillouin-Zone Integrations. *Phys. Rev. B* **1976**, *13*, 5188−5192.
(50) Baldereschi, A. Mean-Value Point in the Brillouin Zone. *Phys. Rev. B* **1973**, *7*, 5212−5215.
(51) Schilling, H.; Camani, M.; Gygax, F. N.; Ruegg, W.; Schenck, A. Depolarisation Studies of Positive Muons in Copper, Vanadium, Niobium And tantalum single crystals. *J. Phys. F* **1982**, *12*, 875−893.
(52) Camani, M.; Gygax, F. N.; Rüegg, W.; Schenck, A.; Schilling, H. Positive Muons in Copper: Detection of an Electric-Field Gradient at the Neighbor Cu Nuclei and Determination of the Site of Localization. *Phys. Rev. Lett.* **1977**, *39*, 836−839.
(53) Clawson, C. W.; Crowe, K. M.; Rosenblum, S. S.; Kohn, S. E.; Huang, C. Y.; Smith, J. L.; Brewer, J. H. Low-Temperature Mobility of Positive Muons in Copper. *Phys. Rev. Lett.* **1983**, *51*, 114−117.
(54) Hartmann, O.; Norlin, L.; Yaouanc, A.; Le Hericy, J.; Karlsson, E.; Niinikoski, T. Low Temperature Studies of Muon Localization in Copper. *Hyperfine Interact.* **1981**, *8*, 533−537.
(55) Flynn, C. P.; Stoneham, A. M. Quantum Theory of Diffusion With Application to Light Interstitials in Metals. *Phys. Rev. B* **1971**, *3*, 2819.
(56) Flynn, C. P.; Stoneham, A. M. Quantum Theory of Diffusion With Application to Light Interstitials in Metals. *Phys. Rev. B* **1970**, *1*, 3966−3978.

DOI: 10.1021/jp5125876
J. Phys. Chem. C XXXX, XXX, XXX−XXX

(57) Teichler, H. On the Theory of Muon Diffusion in Metals. *Phys. Lett. A* **1977**, *64*, 78−80.
(58) Teichler, H. On the Theory of Diffusion of Light Interstitials in Metals. *Hyperfine Interact.* **1979**, *6*, 251−254.
(59) Teichler, H. Microscopic Calculation of Lattice Distortions around μ^+ in Cu. *Phys. Lett. A* **1978**, *67*, 313−315.
(60) Hirata, S.; Miller, E. B.; Ohnishi, Y.-y.; Yagi, K. On the Validity of the BornOppenheimer Separation and the Accuracy of Diagonal Corrections in Anharmonic Molecular Vibrations. *J. Phys. Chem. A* **2009**, *113*, 12461−12469.
(61) Varandas, A.; Xu, Z. Singularities in the Hamiltonian at Electronic Degeneracies. *Chem. Phys.* **2000**, *259*, 173−179.
(62) Sutcliffe, B. T.; Woolley, R. G. Molecular Structure Calculations Without Clamping the Nuclei. *Phys. Chem. Chem. Phys.* **2005**, *7*, 3664−3676.
(63) Takahashi, S.; Takatsuka, K. On the Validity Range of the Born-Oppenheimer Approximation: A Semiclassical Study for All-Particle Quantization of Three-Body Coulomb Systems. *J. Chem. Phys.* **2006**, *124* (144101), 1−14.
(64) Romanowski, Z. B-Spline Solver for One-Electron Schrödinger Equation. *Mol. Phys.* **2011**, *109*, 2679−2691.
(65) Janecek, S.; Krotscheck, E. A Fast and Simple Program for Solving Local Schrödinger Equations in Two and Three Dimensions. *Comput. Phys. Commun.* **2008**, *178*, 835−842.
(66) De Renzi, R. Home Page. http://www.fis.unipr.it/home/roberto.derenzi/dispense/pmwiki.php?n=MuSR.MuonSite (accessed Jan. 26, 2015).

DOI: 10.1021/jp5125876
J. Phys. Chem. C XXXX, XXX, XXX−XXX